



## Comparison of ultra-low-frequency waves at Mercury under northward and southward IMF

Scott A. Boardsen,<sup>1,2</sup> James A. Slavin,<sup>1</sup> Brian J. Anderson,<sup>3</sup> Haje Korth,<sup>3</sup> and Sean C. Solomon<sup>4</sup>

Received 8 June 2009; revised 11 August 2009; accepted 26 August 2009; published 23 September 2009.

[1] Narrow-band ultra-low-frequency (ULF) waves at frequencies greater than the He<sup>+</sup> cyclotron frequency ( $f_{cHe^+}$ ) were detected during MESSENGER's first two Mercury flybys. The waves were observed primarily between closest approach (CA) and the outbound magnetopause. The magnetosphere was very quiet during the first flyby (M1) and highly disturbed during the second flyby (M2); that ULF waves were observed during both flybys despite these different magnetospheric conditions is remarkable. The wave frequency structure in the boundary layer (BL) was similar between M1 and M2. Between CA and the BL, for M1 the wave frequency rose systematically from  $f_{cHe^+}$  to the proton cyclotron frequency ( $f_{cH^+}$ ), while during M2 two frequency bands were observed, one near the He<sup>++</sup> cyclotron frequency and one near  $f_{cH^+}$ . The main difference in the waves between the two flybys, apart from their frequency structure, was their power, which was 4 to 5 times larger during M2 than during M1. **Citation:** Boardsen, S. A., J. A. Slavin, B. J. Anderson, H. Korth, and S. C. Solomon (2009), Comparison of ultra-low-frequency waves at Mercury under northward and southward IMF, *Geophys. Res. Lett.*, 36, L18106, doi:10.1029/2009GL039525.

### 1. Introduction

[2] During the second flyby (M2) of Mercury by the MErcury Surface, Space ENvironment, GEochemistry, and Ranging (MESSENGER) spacecraft on 6 October 2008, bursts of narrow-band ultra-low-frequency (ULF) waves were detected by the Magnetometer almost continuously from closest approach (CA) to the outbound magnetopause (MP) crossing. The interplanetary magnetic field (IMF) was directed southward during this encounter, and the magnetosphere was highly disturbed, with intense reconnection seen at the dayside MP and in the tail [Slavin *et al.*, 2009]. Similar wave observations were made during the spacecraft's first Mercury flyby (M1) on 14 January 2008 [Boardsen *et al.*, 2009]. The IMF was directed northward during M1, however, and magnetospheric activity was minimal [Anderson *et al.*, 2008; Slavin *et al.*, 2008]. The frequency of the ULF waves observed during both encoun-

ters fell primarily between the He<sup>+</sup> cyclotron frequency ( $f_{cHe^+}$ ) and the H<sup>+</sup> cyclotron frequency ( $f_{cH^+}$ ).

[3] The orbital trajectories for M1 and M2 were both nearly in the X-Y plane in Mercury solar orbital (MSO) coordinates. (In MSO coordinates, X is directed from the center of the planet toward the Sun, Z is normal to Mercury's orbital plane and toward the north celestial pole, and Y is in the direction opposite to orbital motion.) The primary difference is that during M1 the spacecraft entered (exited) the magnetosphere at a radial distance of 3.53 (1.87) Mercury radii ( $R_M$ ) and at a sub-solar angle adjusted for aberration of 132° (87°), while for M2 the spacecraft entered (exited) the magnetosphere at a radial distance of 4.14 (1.67)  $R_M$  and at a sub-solar angle of 148° (72°). The similarity in the trajectories coupled with the contrast in magnetic activity during these two encounters provides a unique opportunity to compare ULF wave activity under distinctly different conditions. Here we present ULF wave observations made by the MESSENGER Magnetometer [Anderson *et al.*, 2007] during M2, and we compare these observations with those made during M1.

### 2. Observations

[4] Dynamic spectrograms computed from Magnetometer data, with a sampling rate of 20 s<sup>-1</sup>, over an interval of 20 minutes centered on CA are shown in Figure 1a for M1 and Figure 1b for M2. These spectrograms were created from individual fast Fourier transform (FFT) spectra generated over 15-s intervals, stepping 3.75 s in time from one spectrum to the next. The choice of 15 s reflects a trade-off between frequency resolution and mitigation of ambient magnetic field variability. To more strongly bring out the emission bands for M2, the spectral power matrix for each frequency is the average of the spectral power matrices over that frequency and that of its four nearest neighboring frequencies.

[5] During both flybys, diamagnetic cavities were detected inbound and outbound from CA. The outbound diamagnetic cavities, also termed a boundary layer (BL) by Slavin *et al.* [2008, 2009], were observed during M1 from 19:10:37 to 19:14:14.8 UTC starting at 1.44  $R_M$  and a sub-solar angle of 109° and during M2 from 08:44:26 to 08:49:11 starting at 1.23  $R_M$  and a sub-solar angle of 109°. Within the BL, emission peaks due to ULF waves are clearly visible just above the He<sup>++</sup> cyclotron frequency ( $f_{cHe^{++}}$ ) during both flybys.

[6] A comparison of ULF waves across the boundary-layer transition (BLT) region for M1 and M2 is shown in Figure 2. From Figure 2a it is not clear whether these waves persisted across the BLT during M1, whereas for M2

<sup>1</sup>Heliophysics Science Division, NASA Goddard Space Flight Center, Greenbelt, Maryland, USA.

<sup>2</sup>Goddard Earth Sciences and Technology Center, University of Maryland, Baltimore County, Baltimore, Maryland, USA.

<sup>3</sup>Johns Hopkins University Applied Physics Laboratory, Laurel, Maryland, USA.

<sup>4</sup>Department of Terrestrial Magnetism, Carnegie Institution of Washington, Washington, D. C., USA.

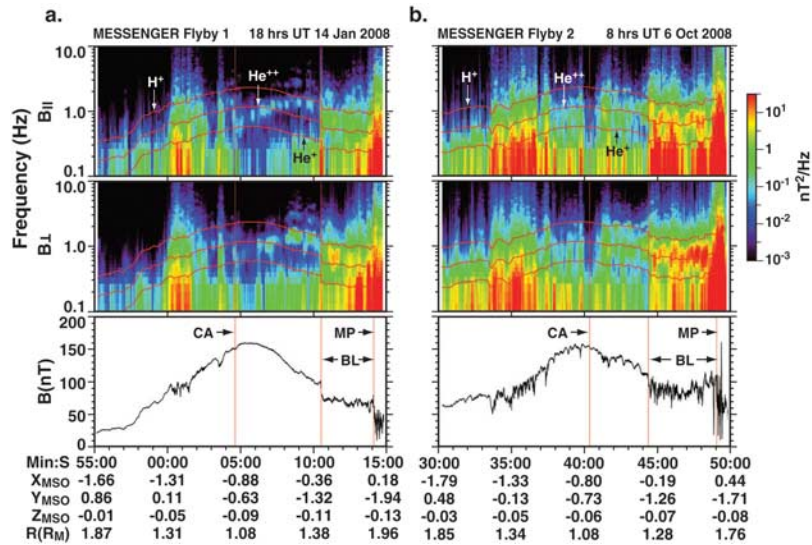


**Figure 1.** Dynamic spectrograms from MESSENGER's (a) first and (b) second flybys of Mercury. From top to bottom are spectrograms of the parallel and perpendicular components and the magnetic field magnitude. The frequency range for the spectrograms is 0.1 to 10 Hz. The red curves show the  $H^+$ ,  $He^{++}$ , and  $He^+$  cyclotron frequencies.

(Figure 2b) the waves were clearly seen across the BLT. The time duration  $\Delta t$  of the steep-gradient portion of the BLT during M1 was only 3 s, however, compared with the wave period near the boundary of  $\sim 1.2$  s. Moreover, the BLT was much sharper during M1 than during M2, a difference that may have affected wave occurrence near the boundary. The scale length  $\frac{B\Delta t}{\Delta B} V_{SAT}$  (where  $V_{SAT}$  is the spacecraft velocity and  $\Delta B$  is the change in magnetic field magnitude  $B$  across the BLT) of the transition region along the spacecraft trajectory is estimated to have been 87 km for M1 and 230 km for M2.

[7] The frequency structure of the ULF emissions between CA and the BL was quite different for M1 and M2. During M1, there was a systematic drift in emission

frequency starting at frequencies just above  $f_{cHe^+}$  and rising to  $f_{cH^+}$  [Boardsen et al., 2009], whereas during M2 two broadband emissions near  $f_{cHe^{++}}$  and  $f_{cH^+}$  were observed with no apparent drift in frequency. Prior to several minutes before CA, no ULF waves in the frequency range between  $f_{cHe^+}$  and  $f_{cH^+}$  could be clearly identified by visual inspection of the time series data, including the inbound diamagnetic cavity, during either M1 or M2.

[8] Representative time series and hodograms of ULF waves, one example between CA and the BL and one in the BL, observed during M2 (see Boardsen et al. [2009, Figure 2] for analogous examples during M1) are shown in Figure 3. The data in the time series plots have been

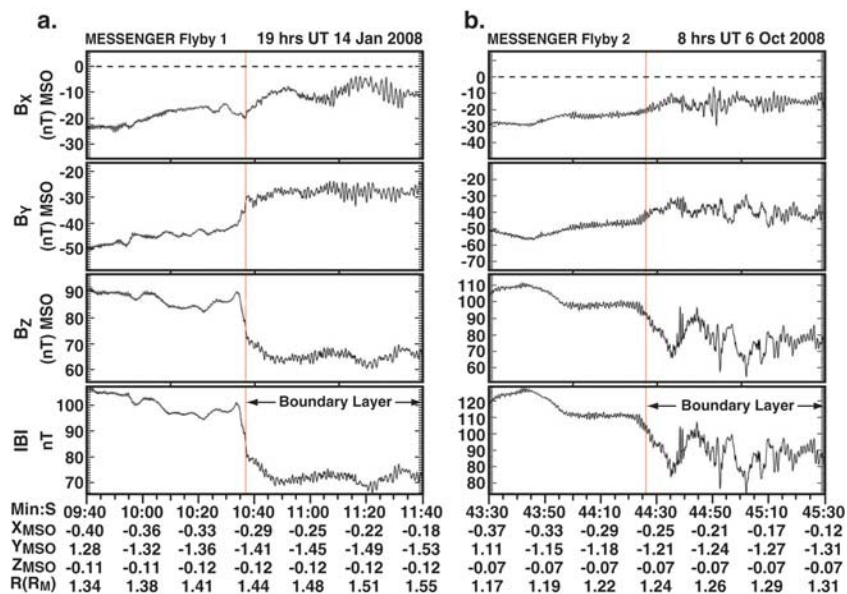


**Figure 2.** Comparison of ULF wave observations across the boundary layer during (a) M1 and (b) M2. During M1, no ULF waves were clearly observed in the transition region, whereas during M2 ULF waves were observed continuously across the transition region (red line).

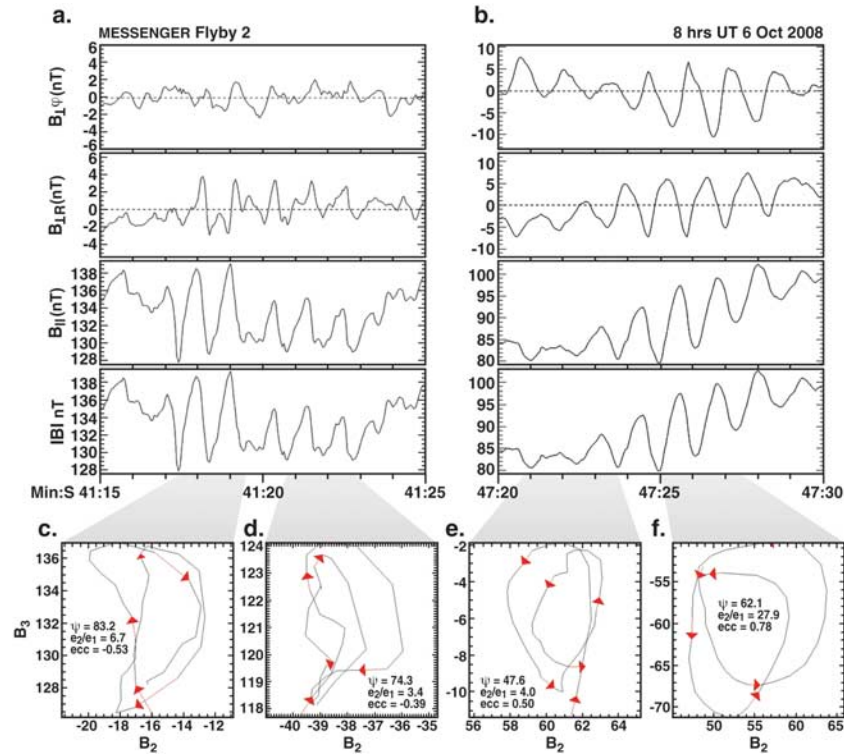


**Figure 3.** (a) Time-series examples of ULF waves detected outbound from closest approach. (b) Example ULF waves in the BL. Hodograms of the time series shown in Figures (c and d) 3a and (e and f) 3b. Axes  $B_2$  and  $B_3$  are the magnetic field in nT projected onto the directions of intermediate and maximum variance, respectively. The wave-normal angle ( $\psi$ ), ratio of median to minimum eigenvalue ( $e_2/e_1$ ), and ellipticity (ecc) are given for each hodogram. The hodogram time intervals are indicated by the shading connecting the hodograms to the time-series plots.

rotated into coordinates perpendicular ( $\perp_\phi$ ,  $\perp_R$ ) and parallel ( $\parallel$ ) to the local magnetic field. The component ( $\perp_\phi$ ) points along the projection of the azimuthal direction onto the perpendicular plane. Figure 3a shows an example of a strong compressional ULF wave occurring close to CA (at 08:40:22 UTC); the period is  $\sim 1$  s and the maximum compressional peak-to-peak amplitude  $\delta B$  (at 08:41:17) is  $\sim 13$  nT (corresponding to a fractional change in magnetic field magnitude  $\delta B/B$  of  $\sim 10\%$ ). Hodograms covering two wave periods for this event are shown in Figures 3c and 3d. The waves are highly elliptical, and their wave vector is nearly perpendicular to the background magnetic field. Between CA and BL during M1, in contrast, the largest peak-to-peak amplitude observed was  $\sim 2$  nT ( $\delta B/B \sim 2\%$ ). During M2 in the BL, the peak-to-peak amplitude within the BL reached a maximum of about 20 nT ( $\delta B/B \sim 25\%$ ), whereas during M1 the maximum peak-to-peak amplitude was  $\sim 10$  nT ( $\delta B/B \sim 15\%$ ). As shown in the hodograms (Figures 3e and 3f), the compressional or transverse nature of the waves was highly variable. At  $\sim 08:47:25$  the wave was primarily compressional, while at  $\sim 08:47:22$  the wave was primarily transverse.

[9] Wave polarization parameters were computed for these ULF waves covering the time period shown in Figures 1a and 1b using the method of Arthur *et al.* [1976]. Briefly, the averaged spectral matrices were diagonalized (using their real parts) by minimum variance analysis. The wave direction is given by the eigenvector corresponding to the minimum eigenvalue ( $e_1$ ). The coherency matrix, the submatrix corresponding to the intermediate

( $e_2$ ) and maximum ( $e_3$ ) eigenvalues, is used to determine the polarization properties.

[10] In our earlier study [Boardsen *et al.*, 2009], events for polarization analysis were selected by visual inspection of time series data. In this paper a different approach was used to select events. A set of polarization parameters were computed from all of the averaged spectral matrices used to create the dynamic spectra shown in Figure 1. The following criteria were applied to select events from this set: (1) the coherency must be greater than 0.75, (2) the ratio of the minimum to the intermediate eigenvalue must be less than 0.5, (3) the Fourier frequency must be at a spectral peak, (4) the spectral peak must be at least two standard deviations above a quadratic fit in log-log space to each spectrum, (5) the power of that peak must be greater than  $0.01 \text{ nT}^2/\text{Hz}$ , (6) the peak frequency computed by fitting a 5-point Gaussian to the spectral peak must lie within the spectral bandwidth (0.067 Hz) of the peak Fourier frequency, and (7) the peak Fourier frequency must lie between  $0.8 f_{CH^+}$  and  $1.2 f_{CH^+}$ . Each selected event is 15 s in duration; because time intervals for dynamic spectra are staggered by 3.75 s there is potentially an overlap between some of the selected events. Such overlap is needed to capture the large variations in polarization properties even within a single wave packet.

[11] Polarization properties of the selected events are shown in Figure 4a for M1 and Figure 4b for M2, and wave properties for the events in Figure 4 are summarized in Table 1. During both flybys, there was a bias toward right-handed polarization, and the wave-normal angle

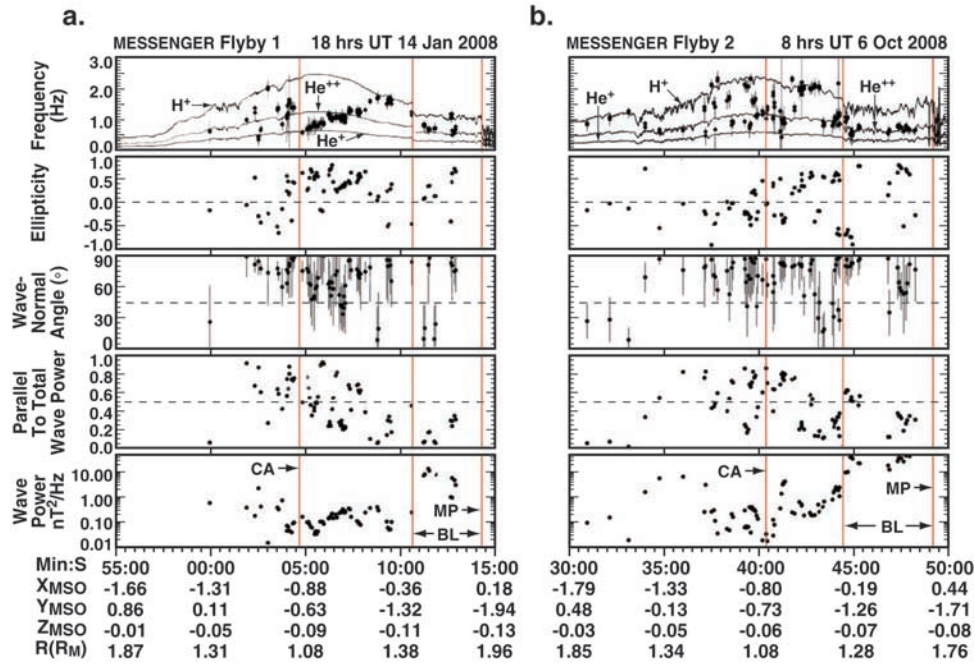


**Figure 4.** Polarization parameters of ULF waves observed during MESSENGER’s (a) first and (b) second flybys of Mercury. The first panels display the frequency of the ULF wave events during each encounter; the solid lines denote  $f_{cH^+}$ ,  $f_{cHe^{++}}$ , and  $f_{cHe^+}$ . The second panels display the ellipticity of the polarization ellipse; positive (negative) ellipticity indicates right- (left-) handed polarization with respect to the ambient magnetic field. The third panels display the wave-normal angle ( $\psi$ ), the angle between the ambient magnetic field and the wave vector. The error estimates for  $\psi$  were derived from the ratio of the minimum to the intermediate eigenvalues and the number of frequencies (5) used to compute the coherency matrix [Khrabrov and Sonnerup, 1998]. The fourth panels show the ratio of the power parallel to the magnetic field to the total power. The fifth panels show the total wave power.

tended to be closer to  $90^\circ$  than  $0^\circ$ . A larger percentage of left-handed waves between CA and the MP was detected during M2 (42%) than M1 (11%). There was also a weak tendency during both flybys for the ratio of the power parallel to the local magnetic field to the total power to decrease outbound from CA. In the BL this ratio can be around 0.3, and for M2 this ratio was greater than 0.5 for 7 of the 19 events.

**Table 1.** Comparison of ULF Wave Properties Between Mercury Flybys M1 and M2<sup>a</sup>

	M <sub>1</sub>				M <sub>2</sub>			
	ALL	<CA	CA-BL	BL	ALL	<CA	CA-BL	BL
$N$	81	17	53	11	86	31	36	19
$f$ (Hz)	1.01	1.17	1.03	0.68	1.02	1.22	1.14	0.74
FWHM (Hz)	0.40	0.48	0.39	0.38	0.44	0.43	0.55	0.40
$ff_{cH^+}$	0.51	0.58	0.45	0.64	0.59	0.71	0.62	0.55
RIGHT HAND	65	8	47	10	39	7	21	11
$\psi > 45^\circ$	67	16	44	7	72	26	28	18
POWER $\parallel \perp$	34	14	20	1	39	17	15	7
$nT^2/Hz$	0.15	0.09	0.13	6.63	0.49	0.18	0.50	33.89
$e_1/e_2$	0.27	0.22	0.28	0.28	0.23	0.24	0.23	0.24

<sup>a</sup>The headings are “ALL” for all events, “<CA” for events before CA, “CA-BL” for events between CA and the BL, and “BL” for events within the BL.  $N$  is the number of events,  $f$  the median frequency, FWHM the median of the full width at half maximum of the spectral peak,  $ff_{cH^+}$  the median of the frequency normalized by  $f_{cH^+}$ , “RIGHT HAND” the number of events that are right handed, “ $\psi > 45^\circ$ ” the number of events for which the wave-normal angle is greater than  $45^\circ$ , “POWER  $\parallel \perp$ ” the number of events for which the parallel power is greater than the perpendicular power, and “ $nT^2/Hz$ ” the median wave power in units of  $nT^2/Hz$ . The quantity  $e_1/e_2$  is the ratio of the minimum to intermediate eigenvalues.

[12] Between CA and the outbound MP, the wave power was clearly larger during M2 than during M1. The ratio of the median wave power between M2 and M1 was 3.8 between CA and the BL and was 5.1 within the BL. The greater wave power during M2 than M1 may be related to the difference in magnetospheric activity, since for the intensely driven system observed during M2 we expect that the magnetosphere was populated by more energetic plasmas and a fraction of this energy ended up in increased plasma wave energy. It should be noted, however, that these flyby observations do not represent a thorough sampling of Mercury’s inner magnetosphere, which will occur only after MESSENGER is in orbit about the planet.

### 3. Discussion

[13] We identify the following salient features of the observations following CA that must be understood: (1) the wave-normal angle is closer to  $90^\circ$  than to  $0^\circ$ , (2) the waves tend to be right handed, (3) the component parallel to the magnetic field is dominant near CA, (3) the frequency structure between CA and the BL is different for southward and northward IMF, (4) the wave power is a factor of  $\sim 5$  higher for southward than for northward IMF, and (5) no waves were observed during the high-latitude third flyby by Mariner 10 [Boardsen et al., 2009]. Field line resonances, cavity modes, and local instabilities have all been proposed as explanations for these waves [Russell, 1989; Glassmeier et al., 2003; Kim and Lee, 2003; Kim et al., 2008; Boardsen et al., 2009].

[14] If the waves are due to a local instability, the tendency for the wave normal to be closer to  $90^\circ$  suggests that this instability is due to the excitation of the fast magnetosonic mode through a loss-cone instability, as briefly suggested by *Boardsen et al.* [2009]. The hybrid simulation of *Trávníček et al.* [2009] shows a large temperature anisotropy near CA, which is due to the large planetary loss cone, and also indicates that the proton density around CA is near the solar wind density. The Fast Imaging Plasma Spectrometer on MESSENGER [*Zurbuchen et al.*, 2008] recorded similar proton counts within the BL during M1 and M2 and higher counts during M2 between CA and the BL [*Anderson et al.*, 2009]. The proton energies were higher during M2 than during M1 [*Anderson et al.*, 2009]. Presumably during southward IMF there was an increased flux of light ions into the inner magnetosphere, and the amplitude of these waves may have increased in correspondence to the greater free energy available. In the light-ion frequency range, these waves would be confined near the equator due to the distortion of the index of refraction by ion-ion resonances. A similar confinement mechanism exists in the Earth's inner equatorial magnetosphere, where the ion-ion resonances are replaced by the lower hybrid resonance and the loss cone source is replaced by proton shell distributions [*Boardsen et al.*, 1992]. For example, at frequencies in the vicinity of the  $\text{He}^{++}\text{-H}^+$  resonance frequency and a wave normal angle of  $80^\circ$ , cold plasma theory (for a background field of 100 nT, an electron density of  $20 \text{ cm}^{-3}$ , and an ion composition of 96% protons and 4%  $\text{He}^{++}$ ) predicts wavelengths in the range of 100 km to 730 km over which there is a large variation in ellipticity (predominately right-handed) and a large variation in the ratio of  $\delta B_{\parallel}$  to  $\delta B_{\perp}$ . The spread in frequency about the ion-ion resonance frequency could be due to Doppler shifts. From *Slavin et al.* [2009], the cross-tail electric field during M2 is estimated to be 2 mV/m, which yields an  $\mathbf{E} \times \mathbf{B}$  drift speed of 20 km/s in a 100-nT magnetic field, so the maximum range in predicted Doppler shifts would be 0.03 to 0.2 Hz. There is a need for theoretical studies of wave generation by loss-cone instabilities and of the propagation of these waves in hot and cold plasmas in Mercury's magnetosphere to determine whether a local generation mechanism is the best candidate for explaining the observed frequencies and polarization properties of these waves.

#### 4. Conclusions

[15] Bursts of narrow-band ULF waves at frequencies primarily between  $f_{c\text{He}^{++}}$  and  $f_{c\text{H}^+}$  were observed almost continuously from shortly before CA to the outbound MP during both of the first two MESSENGER flybys of Mercury. Wave power was  $\sim 5$  times greater during the highly disturbed conditions of M2 than during the quiet conditions of M1. Maximum peak-to-peak wave amplitudes during M2 (M1) were about 10 nT (2 nT) near CA and about 20 nT (10 nT) in the BL. During both flybys, (1) the compressional power relative to the total wave power decreased on average from CA to the MP, (2) the wave-normal angle tended to be closer to  $90^\circ$  than to  $0^\circ$ , and (3) the polarization was primarily right handed. In the BL the frequency peaked just above  $f_{c\text{He}^{++}}$  during both M1

and M2. Between CA and the BL, in contrast, the wave frequencies seen during M2 were split into two bands, one near  $f_{c\text{He}^{++}}$  and one near  $f_{c\text{H}^+}$ , whereas during M1 the frequency drifted systematically from  $f_{c\text{He}^{++}}$  near CA to  $f_{c\text{H}^+}$  near the inner edge of the BL. These waves were detected at similar locations despite very different magnetospheric conditions during the two encounters.

[16] **Acknowledgments.** The MESSENGER project is supported by the NASA Discovery Program under contracts NAS5-97271 to the Johns Hopkins University Applied Physics Laboratory and NASW-00002 to the Carnegie Institution of Washington.

#### References

- Anderson, B. J., M. H. Acuña, D. A. Lohr, J. Scheifele, A. Raval, H. Korth, and J. A. Slavin (2007), The Magnetometer instrument on MESSENGER, *Space Sci. Rev.*, *131*, 417–450, doi:10.1007/s11214-007-9246-7.
- Anderson, B. J., M. H. Acuña, H. Korth, M. E. Purucker, C. L. Johnson, J. A. Slavin, S. C. Solomon, and R. L. McNutt Jr. (2008), The structure of Mercury's magnetic field from MESSENGER's first flyby, *Science*, *321*, 82–85, doi:10.1126/science.1159081.
- Anderson, B. J., et al. (2009), The magnetic field of Mercury, *Space Sci. Rev.*, in press.
- Arthur, C. W., R. L. McPherron, and J. D. Means (1976), A comparative study of three techniques for using the spectral matrix in wave analysis, *Radio Sci.*, *11*, 833–845, doi:10.1029/RS011i010p00833.
- Boardsen, S. A., D. L. Gallagher, D. A. Gurnett, W. K. Peterson, and J. L. Green (1992), Funnel-shaped, low-frequency equatorial waves, *J. Geophys. Res.*, *97*, 14,967–14,976, doi:10.1029/92JA00827.
- Boardsen, S. A., B. J. Anderson, M. H. Acuña, J. A. Slavin, H. Korth, and S. C. Solomon (2009), Narrow-band ultra-low-frequency wave observations by MESSENGER during its January 2008 flyby through Mercury's magnetosphere, *Geophys. Res. Lett.*, *36*, L01104, doi:10.1029/2008GL036034.
- Glassmeier, K.-H., P. N. Mager, and D. Y. Klimushkin (2003), Concerning ULF pulsations in Mercury's magnetosphere, *Geophys. Res. Lett.*, *30*(18), 1928, doi:10.1029/2003GL017175.
- Khrabrov, A. V., and B. U. O. Sonnerup (1998), Error estimates for minimum variance analysis, *J. Geophys. Res.*, *103*, 6641–6651, doi:10.1029/97JA03731.
- Kim, E.-H., and D.-H. Lee (2003), Resonant absorption of ULF waves near the ion cyclotron frequency: A simulation study, *Geophys. Res. Lett.*, *30*(24), 2240, doi:10.1029/2003GL017918.
- Kim, E.-H., J. R. Johnson, and D.-H. Lee (2008), Resonant absorption of ULF waves at Mercury's magnetosphere, *J. Geophys. Res.*, *113*, A11207, doi:10.1029/2008JA013310.
- Russell, C. T. (1989), ULF waves in the Mercury magnetosphere, *Geophys. Res. Lett.*, *16*, 1253–1256, doi:10.1029/GL016i011p01253.
- Slavin, J. A., et al. (2008), Mercury's magnetosphere after MESSENGER's first flyby, *Science*, *321*, 85–89, doi:10.1126/science.1159040.
- Slavin, J. A., et al. (2009), MESSENGER observations of magnetic reconnection in Mercury's magnetosphere, *Science*, *324*, 606–610, doi:10.1126/science.1172011.
- Trávníček, P. M., P. Hellinger, D. Schriver, D. Herčík, J. A. Slavin, and B. J. Anderson (2009), Kinetic instabilities in Mercury's magnetosphere: Three dimensional simulation results, *Geophys. Res. Lett.*, *36*, L07104, doi:10.1029/2008GL036630.
- Zurbuchen, T. H., J. M. Raines, G. Gloeckler, S. M. Krimigis, J. A. Slavin, P. L. Koehn, R. M. Killen, A. L. Sprague, R. L. McNutt Jr., and S. C. Solomon (2008), MESSENGER observations of the composition of Mercury's ionized exosphere and plasma environment, *Science*, *321*, 90–92, doi:10.1126/science.1159314.
- B. J. Anderson and H. Korth, Johns Hopkins University Applied Physics Laboratory, 11100 Johns Hopkins Road, Laurel, MD 20723, USA.  
S. A. Boardsen and J. A. Slavin, Heliophysics Science Division, NASA Goddard Space Flight Center, Mail Stop 674, Greenbelt, MD 20771, USA. (scott.a.boardsen@nasa.gov)  
S. C. Solomon, Department of Terrestrial Magnetism, Carnegie Institution of Washington, 5241 Broad Branch Road, NW, Washington, DC 20015, USA.